# First measurement of coherent $\phi$-meson photoproduction from $^4$He near threshold

T. Hiraiwa,[1,2] M. Yosoi,[1] M. Niiyama,[2] Y. Morino,[3] Y. Nakatsugawa,[4] M. Sumihama,[5] D. S. Ahn,[6] J. K. Ahn,[7] W. C. Chang,[8] J. Y. Chen,[9] S. Daté,[10] H. Fujimura,[11] S. Fukui,[1] K. Hicks,[12] T. Hotta,[1] S. H. Hwang,[13] T. Ishikawa,[14] Y. Kato,[15] H. Kawai,[16] H. Kohri,[1] Y. Kon,[1] P. J. Lin,[8] Y. Maeda,[17] M. Miyabe,[14] K. Mizutani,[2] N. Muramatsu,[14] T. Nakano,[1] Y. Nozawa,[1] Y. Ohashi,[10] T. Ohta,[18] M. Oka,[1] C. Rangacharyulu,[19] S. Y. Ryu,[1] T. Saito,[16] T. Sawada,[20] H. Shimizu,[14] E. A. Strokovsky,[1,21] Y. Sugaya,[1] K. Suzuki,[22] A. O. Tokiyasu,[14] T. Tomioka,[16] T. Tsunemi,[2] M. Uchida,[23] and T. Yorita[1]

(LEPS Collaboration)

[1]*Research Center for Nuclear Physics, Osaka University, Ibaraki, Osaka 567-0047, Japan*
[2]*Department of Physics, Kyoto University, Kyoto 606-8502, Japan*
[3]*High Energy Accelerator Organization (KEK), Tsukuba, Ibaraki 305-0801, Japan*
[4]*Institute of High Energy Physics, Chinese Academy of Sciences, Beijing 100049, China*
[5]*Department of Education, Gifu University, Gifu 501-1193, Japan*
[6]*RIKEN, Nishina Center for Accelerator-Based Science, Wako, Saitama 351-0198, Japan*
[7]*Department of Physics, Korea University, Seoul 02841, Republic of Korea*
[8]*Institute of Physics, Academia Sinica, Taipei 11529, Taiwan*
[9]*Light Source Division, National Synchrotron Radiation Research Center, Hsinchu 30076, Taiwan*
[10]*Japan Synchrotron Radiation Research Institute, Sayo, Hyogo 679-5143, Japan*
[11]*Wakayama Medical University, Wakayama 641-8509, Japan*
[12]*Department of Physics and Astronomy, Ohio University, Athens, Ohio 45701, USA*
[13]*Korea Research Institute of Standards and Science, Daejeon 34113, Republic of Korea*
[14]*Research Center for Electron Photon Science, Tohoku University, Sendai, Miyagi 982-0826, Japan*
[15]*Department of Physics and Astrophysics, Nagoya University, Nagoya, Aichi 464-8602, Japan*
[16]*Department of Physics, Chiba University, Chiba 263-8522, Japan*
[17]*Proton Therapy Center, Fukui Prefectural Hospital, Fukui 910-8526, Japan*
[18]*Department of Radiology, The University of Tokyo Hospital, Tokyo 113-8655, Japan*
[19]*Department of Physics and Engineering Physics, University of Saskatchewan, Saskatoon, Saskatchewan S7N 5E2, Canada*
[20]*Physics Department, University of Michigan, Michigan 48109-1040, USA*
[21]*Joint Institute for Nuclear Research, Dubna, Moscow Region, 142281, Russia*
[22]*Department of Physics, Osaka University, Toyonaka, Osaka 560-0043, Japan*
[23]*Department of Physics, Tokyo Institute of Technology, Tokyo 152-8551, Japan*

(Received 3 November 2017; revised manuscript received 21 January 2018; published 27 March 2018)

The differential cross sections and decay angular distributions for coherent $\phi$-meson photoproduction from helium-4 are measured for the first time at forward angles with linearly polarized photons in the energy range $E_\gamma = 1.685$–$2.385$ GeV. Thanks to the target with spin-parity $J^P = 0^+$, unnatural-parity exchanges are absent, and thus natural-parity exchanges can be investigated clearly. The decay asymmetry with respect to photon polarization is shown to be very close to the maximal value. This ensures the strong dominance (>94%) of natural-parity exchanges in this reaction. To evaluate the contribution from natural-parity exchanges to the forward cross section ($\theta = 0^\circ$) for the $\gamma p \to \phi p$ reaction near threshold, the energy dependence of the forward cross section ($\theta = 0^\circ$) for the $\gamma\,^4\mathrm{He} \to \phi\,^4\mathrm{He}$ reaction is analyzed. The comparison to $\gamma p \to \phi p$ data suggests that enhancement of the forward cross section arising from natural-parity exchanges and/or destructive interference between natural-parity and unnatural-parity exchanges is needed in the $\gamma p \to \phi p$ reaction near threshold.

DOI: 10.1103/PhysRevC.97.035208

## I. INTRODUCTION

The $\phi$-meson photoproduction offers rich information on gluonic interactions at low energies. Because of the almost-pure $s\bar{s}$ components of the $\phi$ meson, meson exchanges in interactions between $\phi$ mesons and nucleons are suppressed by the Okubo-Zweig-Iizuka rule, and multigluon exchanges are expected to be dominant. The slow rise of the total cross section with the energy $\sqrt{s}$ can be well understood by the $t$-channel exchange of gluonic objects with the vacuum quantum numbers, known as the Pomeron trajectory in the Regge phenomenology [1], in the framework of vector-meson dominance [2]. The Pomeron trajectory has been discussed in connection with a glueball trajectory with $J^{\mathrm{PC}} = 2^{++}, 4^{++}, \ldots$, etc. [3–5], but what the physical particles lying on the Pomeron trajectory are is still an open question. While the Pomeron exchange has successfully described the common features of diffractive hadron-hadron and photon-hadron scatterings at high energies

 

[6–8], its applicability to low energies is not completely clear [9,10]. In other hadronic reactions such as $pp$ collisions and photoproduction with flavor changing such as pion or kaon production, it is difficult to study the Pomeron exchange at low energies because meson exchanges become significant. Therefore, $\phi$-meson photoproduction is unique in studying the Pomeron exchange at low energies [11] and searching for a new glueball-associated trajectory, i.e., a daughter Pomeron trajectory [12], as inspired by the scalar glueball ($J^{PC} = 0^{++}$, $M^2 \sim 3$ GeV$^2$) predicted by lattice QCD calculations [13,14].

The LEPS Collaboration measured the $\gamma p \to \phi p$ reaction near threshold at forward angles [15,16], where $t$-channel Pomeron exchange is expected to be dominant. The energy dependence of the forward cross section ($\theta = 0^\circ$) shows a local maximum around $E_\gamma \sim 2$ GeV, which contradicts monotonic behavior as a Pomeron exchange model predicts. This behavior was also observed by CLAS [17,18], whereas the data were obtained by extrapolating from the large-scattering-angle region. Recent measurements by LEPS extended the maximal beam energy from 2.4 to 2.9 GeV and have confirmed an excess from the monotonic curve of a model prediction [19]. Several theoretical models have been proposed so far [10,20–23], but no conclusive interpretation has been obtained yet. From measurements of the $\phi \to K^+K^-$ decay angular distributions with linearly polarized photons [15,24], unnatural-parity exchanges such as $\pi$ and $\eta$ exchanges are known to make a certain contribution (∼30%) near threshold.

Coherent photoproduction with an isoscalar target is very useful for studying the Pomeron exchange at low energies since isovector $\pi$ exchange, which is a dominant meson exchange process, is forbidden [25,26]. The LEPS data for the coherent $\gamma d \to \phi d$ reaction [27] shows that a Pomeron exchange model including a small contribution from the $\eta$ exchange [26] underestimates the energy dependence of the forward cross section ($\theta = 0^\circ$).

In this article, we present the first measurement of the differential cross sections and decay angular distributions for the coherent $\gamma {}^4\mathrm{He} \to \phi {}^4\mathrm{He}$ reaction at forward angles near threshold with linearly polarized photons. This reaction has advantages compared to the $\gamma d$ reaction: First, thanks to the $0^+$ target, this reaction completely eliminates unnatural-parity exchanges since a $0^+$ particle cannot emit an unnatural-parity particle, remaining unchanged in spin and parity, due to spin-parity conservation. Second, owing to the large separation energy of helium-4 nuclei, oherent production events could be cleanly separated from incoherent ones, even better than with a deuterium target. Accordingly, we can investigate natural-parity exchanges such as Pomeron and multigluon exchanges at low energies with better accuracies.

## II. EXPERIMENT AND ANALYSIS

The experiment was carried out at the SPring-8 facility using the LEPS spectrometer [28]. Linearly polarized photons were produced via backward Compton scattering between UV-laser photons with a wavelength of 355 nm and 8-GeV electrons in the storage ring [29]. The photon energy was determined by momentum analysis of the recoil electrons with tagging counters. The photon energy resolution ($\sigma$) was

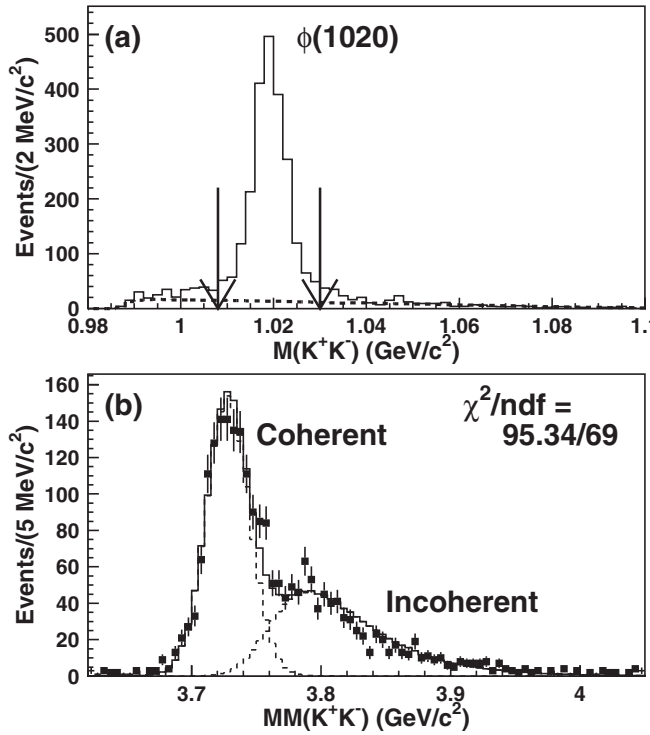


FIG. 1. (a) Invariant mass spectrum for $K^+K^-$ pairs. The dashed curve shows the MC-simulated background. Arrows show cut points for selecting the $\phi$-meson events. (b) Missing mass spectrum for the $^4\mathrm{He}(\gamma, K^+K^-)X$ reaction after selection of the $\phi$-meson events. The solid-line histogram shows the fit result with two MC templates for the coherent and incoherent processes (dashed-line histograms).

13.5 MeV for all energies. The degree of photon polarization varied with the photon energy: 69% at $E_\gamma = 1.685$ GeV and 92% at $E_\gamma = 2.385$ GeV. The systematic uncertainty in the polarization degree was estimated to be less than 0.1%. The tagged photons irradiated a liquid helium-4 target with a length of 15 cm. The integrated flux of the tagged photons was $4.6 \times 10^{12}$. The systematic uncertainty of the photon flux was estimated to be 3%. Produced charged particles were detected at forward angles, and their momenta were analyzed by the LEPS spectrometer. The momentum resolution ($\sigma$) of the spectrometer was 0.9% in $\delta p/p$ for typical 1-GeV/$c$ particles. More details about the experimental setup can be found in Ref. [30].

The production of $\phi$ mesons was identified by the detection of $K^+K^-$ tracks from the $\phi \to K^+K^-$ decay. $K^+K^-$ tracks were selected according to the reconstructed mass-squared and charge by the spectrometer with a $4\sigma$ cut, where $\sigma$ is the momentum-dependent resolution of the reconstructed mass squared. The contamination of pions due to particle misidentifications was reduced to a negligible level by requiring the missing mass of the $^4\mathrm{He}(\gamma, K^+K^-)X$ reaction to be above 3.62 GeV/$c^2$. $K^+K^-$ pairs produced inside the target were selected by imposing a cut on the $z$ positions of the reconstructed vertices of $K^+K^-$ pairs. Under this cut, contamination from materials other than the target was estimated to be 2% with empty-target data. Figure 1(a) shows the invariant mass spectrum for the $K^+K^-$ pairs [M($K^+K^-$)]. A clear

signal for $\phi$ mesons was observed on a small background contribution from nonresonant $K^+K^-$ production. Note that quasifree $K^+\Lambda(1520)$ production followed by $\Lambda(1520) \to K^- p$ decay was found to be negligible in the small momentum transfers $|t|$ of our interest ($-t < 0.2$ GeV$^2$). The $\phi$ meson yields including both coherent and incoherent processes were estimated by fitting invariant mass spectra with Monte Carlo (MC) templates. The spectral shapes for the $\phi$ meson and nonresonant $K^+K^-$ events were reproduced by GEANT3 [31]-based MC simulations, where the geometrical acceptance, the photon energy resolution, the momentum resolution, and the detector efficiencies were implemented. The background level under the $\phi$-meson signal was estimated to be 1%–15%, depending on the photon energy and the momentum transfer.

Coherent events were disentangled from incoherent events by fitting missing mass spectra for the $^4$He$(\gamma, K^+K^-)X$ reaction [MM$(K^+K^-)$] after selecting the $\phi$-meson events as $1.008 < \mathrm{M}(K^+K^-) < 1.030$ GeV$/c^2$ [Fig. 1(b)]. A clear peak for the coherent $\gamma\,^4\mathrm{He} \to \phi\,^4\mathrm{He}$ reaction was observed around MM$(K^+K^-) \approx 3.73$ GeV$/c^2$, corresponding to the mass of helium-4 nuclei. The spectral shapes for the coherent and incoherent processes were reproduced by MC simulations. The missing mass MM$(K^+K^-)$ resolution ($\sigma$) was estimated to be 14–17 MeV$/c^2$, which was consistent with estimates from hydrogen-target data.

To reproduce the line shape of the MM$(K^+K^-)$ spectra for the incoherent process, the Fermi motion and off-shell effects of the target nucleon inside a helium-4 nucleus were simulated as follows: For the off-shell correction, we adopted the first approach in Ref. [27]. The Fermi momenta of the target nucleon were taken from the numerical results of variational Monte Carlo calculations for the helium-4 wave function [32]. Moreover, following Ref. [27], the energy dependence of the forward cross section ($\theta = 0^\circ$) for the $\phi$-meson photoproduction from off-shell nucleons as well as the differential cross section $d\sigma/dt$ was also taken into account.

Systematic uncertainties due to contamination from events other than coherent ones were estimated by considering additional processes, in the MM$(K^+K^-)$ fits, such as

$$\gamma + \text{`}t\text{'} \to \phi + t, \quad \gamma + \text{`}d\text{'} \to \phi + d, \tag{1}$$

where '$t$' ('$d$' stands for the triton (deuteron) wave function in helium-4 nuclei. The off-shell effects of the triton and deuteron clusters inside a helium-4 nucleus were simulated in the same manner as for the incoherent process. Their Fermi momenta were taken from Ref. [32].

The acceptance of the LEPS spectrometer including all the detector efficiencies and the analysis efficiency was calculated using the MC simulation. The detector efficiencies were evaluated from the data channel by channel and were taken into account position dependently in the MC simulation. The simulation was iterated so as to reproduce the measured differential cross section $d\sigma/dt$ and decay angular distributions. The validity of the acceptance calculation as well as the normalization of the photon flux was checked with hydrogen-target data taken in the same period, by comparing the differential cross sections of other reactions with the previous LEPS measurements [15,28,33].

## III. DECAY ANGULAR DISTRIBUTION

First, we present the $\phi \to K^+K^-$ decay angular distributions in the Gottfried-Jackson frame. The three-dimensional decay angular distribution, $W(\cos\Theta, \Phi, \Psi)$, with linearly polarized photons, as a function of the polar ($\Theta$) and azimuthal ($\Phi$) angles of the $K^+$ and the azimuthal angle ($\Psi$) of the photon polarization with respect to the production plane, are parametrized by the nine spin-density matrix elements ($\rho^i_{jk}$) and the degree of photon polarization ($P_\gamma$) [34]. Following Ref. [35], one obtains five one-dimensional decay angular distributions,

$$\begin{aligned}
W(\cos\Theta) &= \frac{3}{2}\left[\frac{1}{2}\left(1-\rho^0_{00}\right)\sin^2\Theta + \rho^0_{00}\cos^2\Theta\right],\\
W(\Phi) &= \frac{1}{2\pi}\left(1 - 2\mathrm{Re}\rho^0_{1-1}\cos 2\Phi\right),\\
W(\Phi-\Psi) &= \frac{1}{2\pi}\left[1 + 2P_\gamma\overline{\rho}^1_{1-1}\cos 2(\Phi-\Psi)\right],\\
W(\Phi+\Psi) &= \frac{1}{2\pi}\left[1 + 2P_\gamma\Delta_{1-1}\cos 2(\Phi+\Psi)\right],\\
W(\Psi) &= 1 - P_\gamma\left(2\rho^1_{11} + \rho^1_{00}\right)\cos 2\Psi,
\end{aligned} \tag{2}$$

where $\overline{\rho}^1_{1-1} \equiv (\rho^1_{1-1} - \mathrm{Im}\rho^2_{1-1})/2$ and $\Delta_{1-1} \equiv (\rho^1_{1-1} + \mathrm{Im}\rho^2_{1-1})/2$. These distributions were measured at $0 < |t| - |t|_{\min} < 0.2$ GeV$^2$ for two photon energy regions ($E1$, $1.985 < E_\gamma < 2.185$ GeV; E2, $2.185 < E_\gamma < 2.385$ GeV), where sufficient statistics were obtained. Here, $|t|_{\min}$ is the minimum $|t|$ for a helium-4 nucleus.

Figures 2(a) and 2(b) show the distribution $W(\cos\Theta)$. The extracted spin-density matrix elements are summarized in Table I. For both the $E1$ and the $E2$ regions, $\rho^0_{00}$ is consistent with 0, which is the same as the values for the $\gamma p$ and $\gamma d$ reactions [15,24]. This indicates the dominance of helicity-conserving processes in the $t$ channel.

The decay asymmetry, $\overline{\rho}^1_{1-1}$, is obtained from $W(\Phi - \Psi)$ [Figs. 2(c) and 2(d)]. It reflects the relative contribution of natural-parity and unnatural-parity exchanges and gives $+0.5(-0.5)$ for pure natural-parity (unnatural-parity) exchanges when helicity conservation holds [34,35]. As shown in Figs. 2(c) and 2(d), quite large oscillations were observed in $W(\Phi - \Psi)$, and therefore a finite bin size could affect the extracted values of $\overline{\rho}^1_{1-1}$ with direct use of Eq. (2). To avoid such finite-bin-size effects, a fit chi-square was defined as

$$\begin{aligned}
\chi^2\left(\overline{\rho}^1_{1-1}, \alpha\right) &= \sum_{i=1}^{N}\frac{(\hat{O}_i - \alpha\hat{E}_i)^2}{\sigma_i^2},\\
\hat{E}_i &= \frac{1}{\Delta x}\int_{\bar{x}_i-\frac{1}{2}\Delta x}^{\bar{x}_i+\frac{1}{2}\Delta x} W(\Phi-\Psi;=x)\,dx,
\end{aligned} \tag{3}$$

where $N$ denotes the number of data points (bins), $\hat{O}_i$ is the number of counts in the $i$th bin, $\alpha$ denotes an overall normalization factor being a free parameter, $\sigma_i$ is the statistical error in the $i$th bin, $\Delta x$ is the bin size, and $\bar{x}_i$ is the mean value of the $i$th bin. We found $\overline{\rho}^1_{1-1}$ to be very close to $+0.5$ for both the $E1$ and the $E2$ regions, indicating almost-pure natural-parity exchanges. However, $\overline{\rho}^1_{1-1}$ sizably deviates from $+0.5$. This

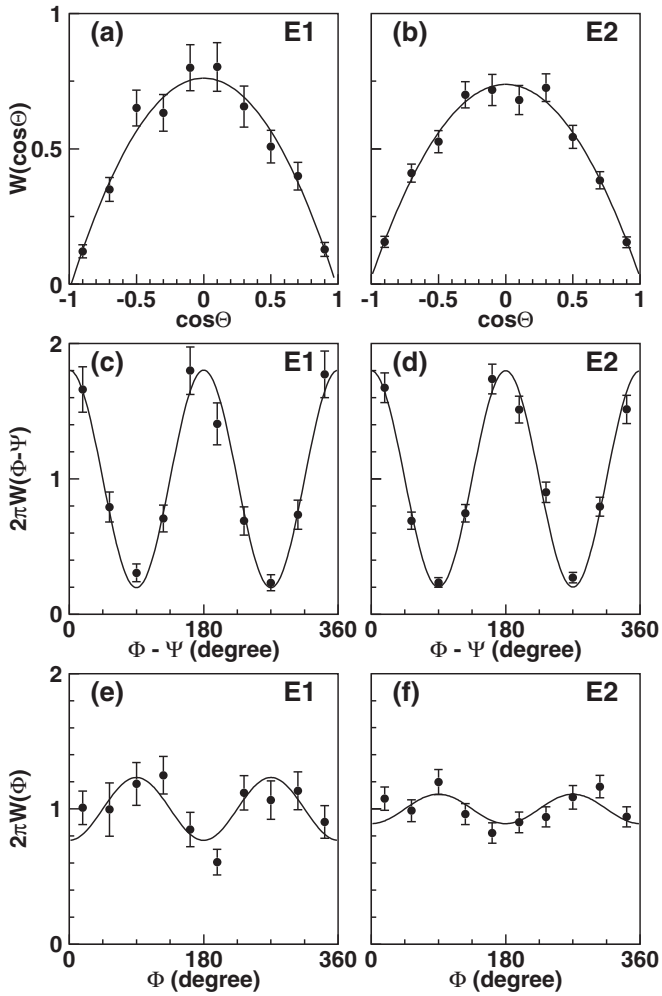


FIG. 2. Acceptance-corrected decay angular distribution for the $\gamma^4$He reaction. $W(\cos\Theta)$ for (a) $E1$ and (b) $E2$. $W(\Phi-\Psi)$ for (c) $E1$ and (d) E2. $W(\Phi)$ for (e) $E1$ and (f) $E2$. Error bars represent statistical errors only. Solid curves are fits to the data by Eqs. (2).

can be understood by the contribution from double helicity-flip transitions from the incident photon to the outgoing $\phi$ meson [35]. In fact, a rather large oscillation of $W(\Phi)$ was observed in the $E1$ region [Fig. 2(e)], giving the spin-density matrix element of $\mathrm{Re}\rho^0_{1-1} \sim 0.11$. This means that the interference of helicity-nonflip and double helicity-flip amplitudes has a nonzero value [36]. A nonzero $\mathrm{Re}\rho^0_{1-1}$ was also observed in the $\gamma p$ [15,19,24] and $\gamma d$ reactions [24]. In particular, the $\mathrm{Re}\rho^0_{1-1}$ obtained here exhibits an energy dependence similar to that in Ref. [15]. Note that the deviation of $\overline{\rho}^1_{1-1}$ is not due to contamination from the incoherent events with $\overline{\rho}^1_{1-1} \approx 0.25$

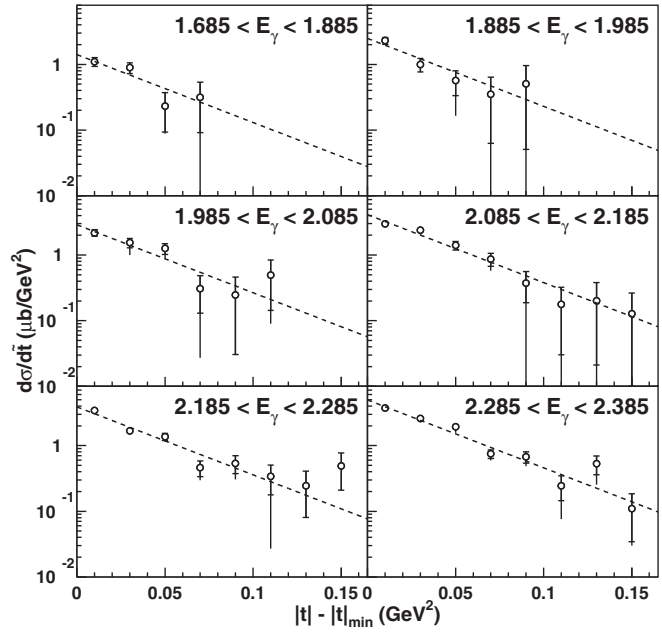


FIG. 3. Differential cross section $d\sigma/d\tilde{t}$ for the $\gamma^4$He reaction. The smaller error bars on the vertical axis represent the statistical error, whereas the larger bars represent the sum of the statistical and systematic errors in quadrature. Dashed curves show the fit results by an exponential function with the common slope $b = 23.81$ GeV$^{-2}$.

[37] because such a deviation does not disappear when a tight mass cut, $\mathrm{MM}(K^+K^-) < 3.72$ GeV/$c^2$, is applied.

## IV. DIFFERENTIAL CROSS SECTION

The differential cross sections as a function of the momentum transfer $\tilde{t}(\equiv|t| - |t|_{\mathrm{min}})$, $d\sigma/d\tilde{t}$, were measured in the energy range $E_\gamma = 1.685$–$2.385$ GeV (Fig. 3). A strong forward-peaking behavior of $d\sigma/d\tilde{t}$ predominantly comes from the helium-4 form factor. To extract the slope of $d\sigma/d\tilde{t}$, the fit was performed with an exponential function, $(d\sigma/dt)_0^{\gamma^4\mathrm{He}} \exp(-b\tilde{t})$, where $(d\sigma/dt)_0^{\gamma^4\mathrm{He}}$ is $d\sigma/d\tilde{t}$ at $t = -|t|_{\mathrm{min}}$ and $b$ the slope parameter. No strong energy dependence of the slope $b$ was found, and the common slope $b$ was determined to be $23.81 \pm 0.95(\mathrm{stat})^{+5.16}_{-0.00}(\mathrm{sys})$ GeV$^{-2}$. The slope $b$ is consistent with a simple estimate from a single-scattering assumption [26], in which the slope $b$ is approximately expressed as $b \approx b_0 + b_F$, where $b_0$ is the slope of the elementary $\gamma p$ reaction ($3.38 \pm 0.23$ GeV$^{-2}$ [15]) and $b_F$ the slope of the squared charge form factor of helium-4 nuclei ($\approx$22 GeV$^{-2}$ [38]). The slope $b$ is also quite reasonable compared with that for other elastic scattering of a hadron off helium-4 in the diffractive regime [39,40]. Note that the systematic error of the slope $b$ comes solely from the

TABLE I. Extracted spin density matrix elements for the $E1$ and $E2$ regions. The first uncertainties are statistical; the second, systematic.

| | $E_\gamma$ range (GeV) | $\rho^0_{00}$ | $\mathrm{Re}\rho^0_{1-1}$ | $\overline{\rho}^1_{1-1}$ | $\Delta_{1-1}$ | $2\rho^1_{11} + \rho^1_{00}$ |
|---|---|---|---|---|---|---|
| $E1$ | 1.985–2.185 | $-0.015 \pm 0.016^{+0.000}_{-0.002}$ | $0.116 \pm 0.030^{+0.000}_{-0.006}$ | $0.454 \pm 0.024^{+0.014}_{-0.000}$ | $-0.111 \pm 0.033^{+0.006}_{-0.000}$ | $0.132 \pm 0.066^{+0.000}_{-0.033}$ |
| $E2$ | 2.185–2.385 | $0.015 \pm 0.012^{+0.002}_{-0.000}$ | $0.054 \pm 0.020^{+0.000}_{-0.004}$ | $0.436 \pm 0.014^{+0.004}_{-0.000}$ | $-0.034 \pm 0.017^{+0.009}_{-0.000}$ | $0.074 \pm 0.041^{+0.011}_{-0.000}$ |

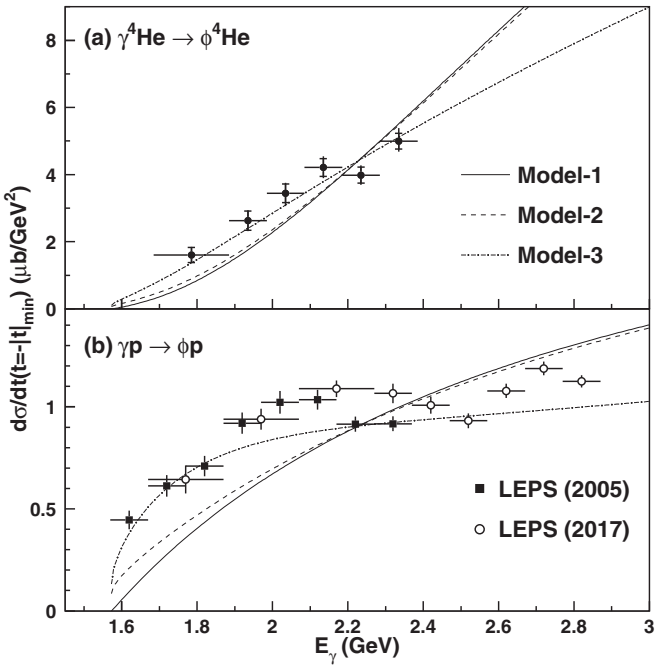


FIG. 4. (a) Energy dependence of $(d\sigma/dt)_0^{\gamma^4\mathrm{He}}$ with the common slope $b = 23.81$ GeV$^{-2}$. The meanings of the error bars are the same as in Fig. 3. Solid, dashed, and dash-dotted curves are the best fits for models 1, 2, and 3 (explained in the text), respectively. (b) Contribution from natural-parity exchanges to the forward cross section ($\theta = 0^\circ$) for the $\gamma p$ reaction with model 1 (solid curve), model 2 (dashed curve), and 3 (dash-dotted curve). Experimental data for the $\gamma p$ reaction are represented by filled squares [15] and open circles [19].

assumption of the additional processes [Eq. (1)] in the MM($K^+K^-$) fits.

Figure 4(a) shows the energy dependence of $(d\sigma/dt)_0^{\gamma^4\mathrm{He}}$ with the common slope $b = 23.81$ GeV$^{-2}$. The differences between the intercepts $(d\sigma/dt)_0^{\gamma^4\mathrm{He}}$ with the fixed (common) and variable (energy-dependent) slopes were found to be within the statistical errors. Also, the systematic errors of $(d\sigma/dt)_0^{\gamma^4\mathrm{He}}$ due to the assumption of the additional processes [Eq. (1)] in the MM($K^+K^-$) fits were found to be small (1.5%–6.5%) compared with the statistical ones, though these are reflected in the final results.

As we shall see, it is difficult to discuss the precise energy dependence of the forward cross section ($\theta = 0^\circ$) for the $\gamma p$ reaction arising from natural-parity exchanges [$\equiv (d\sigma/dt)_0^{\gamma p;\mathrm{NP}}$, where NP denotes the contribution from natural-parity exchanges] directly from the $\gamma^4$He data due to the helium-4 form factor. To evaluate the contribution from natural-parity exchanges to the $\gamma p$ reaction, we constructed three models for the energy dependence of $(d\sigma/dt)_0^{\gamma p;\mathrm{NP}}$, where their overall strengths are unknown and to be determined. The first one (model 1) is simple; that is, $(d\sigma/dt)_0^{\gamma p;\mathrm{NP}}$ increases with the energy as $(k_\phi/k_\gamma)^2$ [41], where $k_\phi$ ($k_\gamma$) is the 3-momentum of $\phi$ mesons (photons) in the center-of-mass frame. The second one (model 2) is a conventional Pomeron exchange model as in Ref. [26]. The third one (model 3) describes a threshold enhancement in the energy dependence of $(d\sigma/dt)_0^{\gamma p;\mathrm{NP}}$. This could be realized by modifying the conventional Pomeron exchange model and/or a manifestation of additional natural-parity exchanges near threshold. For model 3, we used the Pomeron and daughter Pomeron exchange model in Ref. [10]. The relative contribution from the daughter Pomeron exchange was adjusted so as to fit the available low-energy $\gamma p$ data [15,18,19].

A theoretical calculation for the coherent $\gamma d$ reaction has been done by Titov *et al.* [26], in which they describe the forward cross section by using the amplitudes for the elementary $\gamma p$ reaction and the deuteron form factor. Similarly, $(d\sigma/dt)_0^{\gamma^4\mathrm{He}}$ is described by using the charge form factor for helium-4 ($|F_C|^2$) [38] as

$$\left(\frac{d\sigma}{dt}\right)_0^{\gamma^4\mathrm{He}} = 16|F_C|^2\left(\frac{d\sigma}{dt}\right)_0^{\gamma p;\mathrm{NP}}. \quad (4)$$

Here, $|F_C|^2$ is evaluated at $t = -|t|_{\mathrm{min}}$. To fix the overall strengths for the above models, we used this relation in the fit to the $\gamma^4$He data with the overall strengths as free parameters. The best fits for models 1, 2, and 3 are depicted in Fig. 4(a) as solid, dashed, and dash-dotted curves, respectively. The $\chi^2$/ndf's are 48.8/5, 39.8/5, and 10.2/5 for models 1, 2, and 3, respectively.

Figure 4(b) shows the contribution from natural-parity exchanges to the forward cross section ($\theta = 0^\circ$) for the $\gamma p$ reaction with each model, together with the experimental data from LEPS [15,19]. Models 1 and 2 gave similar results, and we found both curves to be slightly above the data points for $E_\gamma > 2.4$ GeV. On the other hand, the experimental data on the decay asymmetry $\overline{\rho}^1_{1-1}$ [19] show a sizable, 20%–30%, contribution from unnatural-parity exchanges to the forward cross section for $2.4 < E_\gamma < 2.9$ GeV. This suggests that destructive interference between natural-parity and unnatural-parity exchanges is needed to explain the measurements of both the forward cross section and the decay asymmetry. In contrast to models 1 and 2, model 3 describes the experimental data fairly well. For $E_\gamma > 1.9$ GeV, we found the curve to be below the data by ∼20%, except for a few data points. This can be compensated by the observed 20%–40% contribution from unnatural-parity exchanges [15,19,24]. In this case, large interference effects between natural-parity and unnatural-parity exchanges are not needed, which is compatible with our current understanding that the interference effect between Pomeron and $\pi$ exchanges would be small [2,10]. Note that destructive interference between natural-parity and unnatural-parity exchanges is also needed for $E_\gamma < 1.9$ GeV because simply adding the unnatural-parity contribution (∼30%) overestimates the experimental data.

## V. CONCLUSION

In conclusion, we have presented the first measurement of the differential cross sections and decay angular distributions for coherent $\phi$-meson photoproduction from helium-4 at forward angles with linearly polarized photons in the energy range $E_\gamma = 1.685$–$2.385$ GeV. With the elimination of unnatural-parity exchanges, this reaction provides a unique and clean way of investigating natural-parity exchanges in $\phi$-meson photoproduction at low energies. The measurement

of $\overline{\rho}^1_{1-1}$ demonstrates the strong dominance (>94%) of natural-parity exchanges in this reaction. Three models were constructed for describing the contribution from natural-parity exchanges to the forward cross section ($\theta = 0^\circ$) for the $\gamma p$ reaction near threshold, and their overall strengths were determined from the present data. The comparison of them to available $\gamma p$ data suggests that enhancement of the forward cross section arising from natural-parity exchanges and/or destructive interference between natural-parity and unnatural-parity exchanges is needed in the $\gamma p$ reaction near threshold. Further theoretical and experimental efforts will be of great help in revealing the underlying reaction mechanisms in $\phi$-meson photoproduction at low energies.

## ACKNOWLEDGMENTS

The authors thank the staff at SPring-8 for supporting the LEPS experiment. We thank A. I. Titov, A. Hosaka, and H. Nagahiro for fruitful discussions. The experiment was performed at the BL33LEP of SPring-8 with the approval of the Japan Synchrotron Radiation Research Institute (JASRI) as a contract beamline (Proposal No. BL33LEP/6001). This work was supported in part by the Ministry of Education, Science, Sports and Culture of Japan, the National Science Council of the Republic of China (Taiwan), the National Science Foundation (USA), and the National Research Foundation (Korea).

[1] P. D. B. Collins, *An Introduction to Regge Theory and High-Energy Physics* (Cambridge University Press, Cambridge, UK, 1977).
[2] T. H. Bauer, R. D. Spital, D. R. Yennie, and F. M. Pipkin, Rev. Mod. Phys. **50**, 261 (1978).
[3] P. V. Landshoff, arXiv:hep-ph/9410250.
[4] L. S. Kisslinger and W.-H. Ma, Phys. Lett. B **485**, 367 (2000).
[5] F. J. Llanes-Estrada, S. R. Cotanch, P. J. de A. Bicudo, J. E. F. T. Ribeiro, and A. Szczepaniak, Nucl. Phys. A **710**, 45 (2002).
[6] A. Donnachie and P. V. Landshoff, Nucl. Phys. B **267**, 690 (1986).
[7] A. Donnachie and P. V. Landshoff, Phys. Lett. B **185**, 403 (1987).
[8] M. A. Pichowsky and T.-S. H. Lee, Phys. Rev. D **56**, 1644 (1997).
[9] R. A. Williams, Phys. Rev. C **57**, 223 (1998).
[10] A. I. Titov, T.-S. H. Lee, H. Toki, and O. Streltsova, Phys. Rev. C **60**, 035205 (1999).
[11] V. Barger and D. Cline, Phys. Rev. Lett. **24**, 1313 (1970).
[12] T. Nakano and H. Toki, in *Proceedings of the International Workshop on Exciting Physics with New Accelerator Facilities, SPring-8, Hyogo, 1997* (World Scientific, Singapore, 1998) p. 48.
[13] C. J. Morningstar and M. Peardon, Phys. Rev. D **60**, 034509 (1999).
[14] A. Vaccarino and D. Weingarten, Phys. Rev. D **60**, 114501 (1999).
[15] T. Mibe *et al.*, Phys. Rev. Lett. **95**, 182001 (2005).
[16] S. Y. Ryu *et al.*, Phys. Rev. Lett. **116**, 232001 (2016).
[17] B. Dey *et al.*, Phys. Rev. C **89**, 055208 (2014).
[18] H. Seraydaryan *et al.*, Phys. Rev. C **89**, 055206 (2014).
[19] K. Mizutani *et al.*, Phys. Rev. C **96**, 062201(R) (2017).
[20] S. Ozaki, A. Hosaka, H. Nagahiro, and O. Scholten, Phys. Rev. C **80**, 035201 (2009); **81**, 059901(E) (2010).
[21] A. Kiswandhi and S. N. Yang, Phys. Rev. C **86**, 015203 (2012); **86**, 019904(E) (2012).
[22] H.-Y. Ryu, A. I. Titov, A. Hosaka, and H.-C. Kim, Prog. Theor. Exp. Phys. **2014**, 023D03 (2014).
[23] R. F. Lebed, Phys. Rev. D **92**, 114006 (2015).
[24] W. C. Chang *et al.*, Phys. Rev. C **82**, 015205 (2010).
[25] A. I. Titov, M. Fujiwara, and T. S.-H. Lee, Phys. Rev. C **66**, 022202(R) (2002).
[26] A. I. Titov and B. Kämpfer, Phys. Rev. C **76**, 035202 (2007).
[27] W. C. Chang *et al.*, Phys. Lett. B **658**, 209 (2008).
[28] M. Sumihama *et al.*, Phys. Rev. C **73**, 035214 (2006).
[29] N. Muramatsu *et al.*, Nucl. Instrum. Methods Phys. Res., Sec. A **737**, 184 (2014).
[30] Y. Morino *et al.*, Prog. Theor. Exp. Phys. **2015**, 013D01 (2015).
[31] R. Brun and F. Carminati, CERN Program Library Long Writeup Report No. W5013 (1993).
[32] R. B. Wiringa, R. Schiavilla, S. C. Pieper, and J. Carlson, Phys. Rev. C **89**, 024305 (2014).
[33] M. Sumihama *et al.*, Phys. Lett. B **657**, 32 (2007).
[34] K. Schilling, P. Seyboth, and G. Wolf, Nucl. Phys. B **15**, 397 (1970).
[35] A. I. Titov and T.-S. H. Lee, Phys. Rev. C **67**, 065205 (2003).
[36] J. Ballam *et al.*, Phys. Rev. D **7**, 3150 (1973).
[37] W. C. Chang *et al.*, Phys. Lett. B **684**, 6 (2010).
[38] R. B. Wiringa, Phys. Rev. C **43**, 1585 (1991).
[39] Ableev V. G. *et al.*, Yad. Fiz. **36**, 1434 (1982) [Sov. J. Nucl. Phys. **36**, 834 (1982)].
[40] Ableev V. G. *et al.*, Yad. Fiz. **34**, 769 (1981) [Sov. J. Nucl. Phys. **34**, 428 (1981)].
[41] D. P. Barber *et al.*, Z. Phys. C **12**, 1 (1982).